Doping of cobalt oxide with transition metal impurities: *Ab initio* study

P. A. Ignatiev,[1] N. N. Negulyaev,[2] D. I. Bazhanov,[1,3] and V. S. Stepanyuk[1]
[1]*Max-Planck-Institut für Mikrostrukturphysik, Weinberg 2, D-06120 Halle/Saale, Germany*
[2]*Fachbereich Physik, Martin-Luther-Universität Halle-Wittenberg, Friedemann-Bach-Platz 6, D-06099 Halle/Saale, Germany*
[3]*Faculty of Physics, Moscow State University, 119899 Moscow, Russia*
(Received 30 June 2009; revised manuscript received 3 June 2010; published 18 June 2010)

We present an *ab initio* study of structural, electronic, and magnetic properties of rocksalt cobalt oxide doped with 3*d* transition metal atoms (Mn, Fe, and Ni). Our calculations are based on the generalized gradient approximation to the density-functional theory corrected for on-site Coulomb interaction (GGA+*U*). Different *ab initio* approaches based on the plane-wave basis set are applied. Structural and magnetic characteristics of pure CoO are calculated and compared with available experimental and theoretical results. Magnetic states of single impurities in CoO are revealed. The interaction between impurities is discussed. Our study demonstrates that both single impurities and their pairs do not break the type-II antiferromagnetic order of the host CoO.

DOI: 10.1103/PhysRevB.81.235123 PACS number(s): 71.27.+a, 71.15.Mb, 71.55.−i

I. INTRODUCTION

It was realized a long-time ago that transition metal oxides (TMO) exhibit a vast variety of properties which can be exploited in technology.[1,2] Despite a growing interest in structural, elastic, electrical, and magnetic properties of TMO, descriptions of band structures of insulating TMOs within existing theoretical models were not quite acceptable.[1] The main difficulty arises from the fact, that the valence bandwidth of *d* electrons and their effective on-site Coulomb interaction are of comparable value.[3] Any electron transfer between transition metal ions is, therefore, accompanied by large energy fluctuations and as a result *d* electrons of a TMO can neither be described by collective nor by localized electron models and need a special treatment. In particular, 3*d* TMOs with NaCl crystal structure (which we are interested in) were revealed experimentally to be insulators[3,4] while conventional density-functional theory calculations result in strongly reduced or even vanished gaps between valence and conduction bands.[5–7]

The onset of a wide range of theoretical treatments of TMOs was caused, on the one hand, by the rising interest in semiconducting TMOs as possible components of various microelectronic devices, and, on the other hand, by the invention of a rather simple but efficient approximation based on the Hubbard model.[8–13] In this approach, correlation effects in the electronic structure of a TMO are introduced as a correction (+*U*) to the total energy functional, i.e., by inclusion of a repulsive Coulomb potential from the Hubbard model into the density-functional theory in local-spin-density approximation (LSDA) or generalized gradient approximation (GGA).[8] Various studies have clearly demonstrated the validity of this approach: LSDA+*U* and GGA+*U* calculations can reasonably well describe the crystal structure of TMO, their electronic structure and magnetic properties.[8,13,14] The +*U* formalism is a convenient tool for studying various ways of tuning magnetic, piezoelectric, optical, and semiconducting properties of TMOs. One of the most common path to such a tuning lies in doping TMOs by impurities. Classical examples of doped systems are ZnO-based dilute semiconductors,[15–19] various perovskites,[20] and TMOs with NaCl crystal structure.[2,21]

In this work we focus on the CoO in NaCl crystal structure with a type-II antiferromagnetic state (AF-II) magnetic order doped with 3*d* metal impurities. All presented results are obtained by means of the *ab initio* GGA+*U* calculations performed using several computer codes. We reinvestigate the electronic structure of CoO and describe magnetic coupling between Co ions within the Heisenberg model. Our primary goal, however, is to reveal how 3*d* impurities are coupled to the host CoO oxide and to each other. We demonstrate the invariability of the AF-II magnetic order in presence of impurities and show that impurities do not form compact arrangements inside the host.

The rest of the paper is organized as follows. In Sec. II we describe the methodology of the GGA+*U* and overview the details of *ab initio* procedures involved. Section III is devoted to obtained results. At first we present the optimized crystal structure of CoO. Then we consider a Co spin-flip impurity and estimate from our *ab initio* results Heisenberg exchange constants of Co^{2+} ions. After that we turn to Mn, Fe, and Ni single impurities in CoO. The section is closed by a discussion. In Sec. IV we present our results on pairs of magnetic impurities.

II. COMPUTATIONAL DETAILS

A. GGA+*U* method

Strong on-site Coulomb correlation effects typical for TMO were considered in our work within the corrected generalized gradient approximation to the density-functional theory. In this formalism the on-site Coulomb interaction $E_{Hub}[n^{\sigma}_{i,m}]$ is added to the total energy functional $E_{\mathrm{GGA}}[n^{\sigma}(\mathbf{r})]$ for electrons with spin σ occupying orbital $|l,m\rangle$ of atom i. Since a part of such Hubbard-type interaction is already included in E_{GGA} on an average way, double counting correction E_{dc} has to be subtracted from the total energy, thus giving the following expression:

$$E_{\mathrm{GGA}+U}[n^{\sigma}(\mathbf{r})] = E_{\mathrm{GGA}}[n^{\sigma}(\mathbf{r})] + E_{Hub}[n^{\sigma}_{i,m}] - E_{dc}[n^{\sigma}_{i,l}]. \quad (1)$$

The functional Eq. (1) can be simplified by means of the mean-field approximation involving spherically averaged,

m-independent screened Coulomb interaction U, and exchange energy $\mathcal{J}$ (Refs. 8, 11–13, and 22):

$$E_{Hub}[n^{\sigma}_{i,m}] = \sum_{i,l} \frac{U_{i,l}}{2} \sum_{\sigma,m,m'} n^{\sigma}_{i,m} n^{-\sigma}_{i,m'} + \sum_{i,l} \frac{U_{i,l} - \mathcal{J}_{i,l}}{2} \sum_{\sigma,m \neq m'} n^{\sigma}_{i,m} n^{\sigma}_{i,m'}. \quad (2)$$

In the atomic (or full localized) limit when orbital occupation numbers $n^{\sigma}_{i,m}=0$ or 1, the double counting term E_{dc} can be written as[22]

$$E_{dc}[n^{\sigma}_{i,l}] = \sum_{i,l} \frac{U_{i,l}}{2} N_{i,l}(N_{i,l}-1) - \sum_{i,l} \frac{\mathcal{J}_{i,l}}{2} \sum_{\sigma} N^{\sigma}_{i,l}(N^{\sigma}_{i,l}-1), \quad (3)$$

where $N^{\sigma}_{i,l}=\Sigma_m n^{\sigma}_{i,m}$ is the number of electrons with the given spin projection at the orbital l and $N_{i,l}$ is the total occupation number of this orbital. The total energy in Eq. (1) is expressed as

$$E_{\mathrm{GGA}+U} = E_{\mathrm{GGA}} + \sum_{i,l} \frac{U_{i,l} - \mathcal{J}_{i,l}}{2} \sum_{\sigma} [Tr(n^{\sigma}_{i,l}) - Tr(n^{\sigma}_{i,l} n^{\sigma}_{i,l})]. \quad (4)$$

In our case the GGA+U approach is applied to d electrons ($l=2$) at transition metal sites i. Note that rotationally invariant total-energy functional $E_{\mathrm{GGA}+U}$ depends on the external non-*ab initio* numerical parameter $U^{i,l}_{eff}=U_{i,l}-\mathcal{J}_{i,l}$.[8,11–13,22] In the limit of $U^{i,l}_{eff} \to 0$ the GGA+U approach turns into the standard GGA. Additional inconveniences arise from the fact that in a many-body system elements $n^{\sigma}_{i,mm'}$ of the density matrix can be defined within the GGA+U by means of the quasiparticle wave functions $\psi^{\sigma}_{\mathbf{k}v}$ of the valence states ($\mathbf{k}v$) and the corresponding occupation numbers $f^{\sigma}_{\mathbf{k}v}$ only in general form[13]

$$n^{\sigma}_{i,mm'} = \sum_{\mathbf{k}v} f^{\sigma}_{\mathbf{k}v} \langle \psi^{\sigma}_{\mathbf{k}v} | \mathcal{P}_{i,mm'} | \psi^{\sigma}_{\mathbf{k}v} \rangle, \quad (5)$$

where projector $\mathcal{P}_{i,mm'}$ can be constructed in a number of equivalently applicable ways and none of them can be stated to be the uniquely correct one.[13]

To avoid a dependence of our results on the details of the formulation several *ab initio* codes were involved in the study. We used two different plane-wave (PW) pseudopotential (PP) codes: Vienna *ab initio* simulation package (VASP) (Refs. 23–25) and QUANTUM ESPRESSO (QE).[26,27] Calculations for bulk cobalt oxide have also been verified by means of WIEN2K full-potential (FP) linearized augmented PW (LAPW) code.[28] The spherically averaged GGA+U double counting correction [Eq. (3)] was used in all three cases (VASP—Ref. 12; QE—Ref. 13; and WIEN2K—Refs. 8, 11, and 22).

B. Details of the calculations

All the calculations were performed using the GGA+U formalism. The equilibrium lattice parameters were determined by the optimization of the structure of the unit cell built of 12 atoms, which is shown in Fig. 1(a). Impurities were incorporated into larger 108-atom supercells constructed of $3\times3\times1$ original unit cells [Fig. 1(b)]. The Monkhorst-Pack (MP) (Ref. 29) **k**-point mesh generation method was applied in all calculations. Below we present a survey of the most important parameters of the methods used.

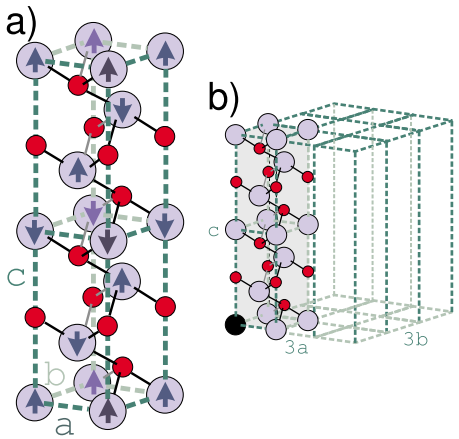

FIG. 1. (Color online) (a) The unit cell used in calculations. Co and O atoms are sketched with large light blue circles and small red circles, respectively. Atomic planes defined by Bravais vectors **a** and **b** correspond to {111} planes of the cubic $Fm\bar{3}m$ structure. Arrows on Co atoms depict mutual alignment of magnetic moments, thus showing AF-II structure of the cell. (b) A large supercell built of $3\times3\times1$ unit cells. The black circle shows the position of an impurity.

1. VASP

GGA exchange-correlation functional was used in the form suggested by Perdew *et al.* (GGA-PW91).[30] Calculations were performed by means of projector-augmented wave (PAW) pseudopotentials[25] with the following configurations for valence electrons of Fe, Co, Ni, and O, respectively: ($3d^74s^1$), ($3d^84s^1$), ($3d^94s^1$), and ($2s^22p^4$). Expansion for the plane-wave basis set was limited by a cut-off energy of 500 eV. The MP $20\times20\times4$ **k**-point mesh was found to be optimal for the 12-atom unit cell [Fig. 1(a)]. In larger 108-atom supercells the MP **k**-point mesh was reduced to $5\times5\times3$. The same sampling was employed in calculations of density of states (DOS). The Gaussian broadening of 0.1 eV was applied both in self-consistent and DOS calculations. The on-site Coulomb repulsion U^{Co}_{eff} for Co d electrons was set to 6.1 eV. This value has been reported to reproduce in VASP calculations the experimental energy gap of CoO.[31]

2. Quantum Espresso

In this PW-PP method[26] we used the Perdew-Burke-Ernzerhof (PBE) GGA (Ref. 32) exchange-correlation functional and ultrasoft PPs (US PPs). The configurations of the valence electrons of Fe, Co, Ni, and O were the same as in the case of VASP. Valence configuration of pseudopotentials chosen for Mn impurity is ($3s^23p^64s^23d^5$) (Ref. 27). We

checked the convergence of structural and electronic properties of bulk CoO as a function of wave-function and electronic density cut-off energies E_{WF} and E_ρ and arrived at the conclusion that it is enough to set E_{WF}=40 Ry and E_ρ =200 Ry. It is important to note that these small values can be used only if the projector on the Löwdin orthogonalized atomic orbitals[33] is used for the calculations of the density matrix $n^\sigma_{i,l}$. According to our tests this option allows also to use less dense MP **k**-point meshes: $10\times10\times3$ for the small supercell and $3\times3\times2$ for large ones. To facilitate the convergence of the self-consistent iterations we applied to bands the Methfessel-Paxton spreading[34] with the half width of 0.004 Ry. To find U_{eff} we performed calculations based on the linear-response approach according to the scheme proposed by Cococcioni and de Gironcoli.[13] The resulting value of 4.5 eV is smaller than those used in VASP calculations but it is close to 4.3 and 4.6 eV obtained for FeO and NiO by means of the same method.[13] The difference between U_{eff} used in VASP and QE could be explained by two major reasons. The first is that U_{eff} is pseudopotential dependent. VASP and QE exploit in our case even different types of pseudopotentials: PAW in VASP and US in QE. The second reason concerns calculations of orbital occupation numbers $n_{i,m}$. In VASP, occupation numbers are calculated by means of a projection onto localized atomic orbitals and only wave functions of the same atom are orthogonal by construction. Hence, there could be overlap regions in between atoms. In QE atomic wave functions belonging to different atoms are orthogonalized by Löwdin projector, which actually means that spatial charge distributions are taken into account in $n_{i,m}$ calculations differently in VASP and QE.

3. WIEN2k

This full-potential linearized augmented plane-wave method[28] was applied to verify the results of PP methods on the bulk cobalt oxide. Parameters of calculations were taken from Ref. 14. In particular, we used U^{Co}_{eff}=6.88 eV; the smallest of the atomic sphere radii R_{MT} and the plane-wave cut-off parameter K_{max} were chosen as $R_{MT}\cdot K_{max}$=8. The GGA-PBE exchange-correlation functional was applied. The Fermi energy is calculated using Blöhl tetrahedron *k*-space integration method. The maximum charge density cutoff G_{max} is 12 $\mathrm{Ry}^{0.5}$.

III. RESULTS AND DISCUSSION

A. Pure CoO

Paramagnetic CoO has the NaCl structure described by the space group $Fm\bar{3}m$.[35,36] Very often another, magnetic state of CoO is in the focus of research: a AF-II exists below the Néel temperature T_N=290 K.[35] In this structure magnetic moments of Co within same {111} sheet of a cubic cell are aligned parallel to each other but antiparallel to the moments in adjacent sheets, so the magnetic propagation vector $\mathbf{Q}_{\mathrm{II}}$ in the cubic unit cell of AF-II structure is [0.5,0.5,0.5]. Recent high-resolution x-ray diffraction studies[35,36] revealed tetragonal distortion along the edges of the $Fm\bar{3}m$ unit-cell cube with c/a=0.988 accompanied by a small trigonal deformation along the [111] direction.[35] These lattice distortions change the crystal symmetry from tetragonal to monoclinic with an angle of 89.962° between the two edges of a different length.

TABLE I. Lattice parameters $a\equiv b$ (Å), c (Å), spin magnetic moments m_S (μ_B), and fundamental band-gap values Δ (eV) calculated by various *ab initio* methods and measured experimentally.

	$a\equiv b$	c	m_S	Δ
QE[a,b]	3.07	14.81	2.60	2.5
QE[c,b]	3.05	14.951	2.63	2.5
VASP[a,b]	3.04	14.76	2.76	2.8
VASP[c,b]	3.04	14.89	2.77	2.7
VASP[a,d]	3.03[e]	14.71[e]	2.74	2.7
WIEN2K[a,b]	3.08	14.96	2.77	2.6
WIEN2K[c,f]	3.05	14.96[e]	2.66	2.1
Experiment[g,h]	3.01	14.76[e]		2.6

[a]Distorted unit cell.
[b]This work.
[c]Ideal unit cell, $c=a\sqrt{24}$.
[d]Reference 31.
[e]Calculated from the given structure.
[f]Reference 14.
[g]Reference 35.
[h]Total magnetic moment of Co is $3.98\mu_B$, orbital magnetic moment $\simeq1\mu_B$ (Refs. 14 and 31).

In GGA+U structure optimization, cubic $Fm\bar{3}m$ unit cell of CoO exhibits small rhombohedral distortion along [111] direction, so the symmetry of the unit cell is changed to $R\bar{3}m$.[31] Such a rhombohedral distortion has not been detected experimentally and it presumably is an artifact of the method. To avoid possible misleading results caused by this distortion we considered both ideal and distorted structures.

It is convenient for us to use a hexagonal unit cell defined by two Bravais vectors **a** and **b** lying in the {111} plane of the $Fm\bar{3}m$ unit cell. In this case the third vector **c** defines the position of the next layer of atoms with an equivalent stacking and magnetization direction. Such a structure is sketched in Fig. 1(a). If $a\equiv b$, γ=60°, $\alpha=\beta$=90°, and $c=a\sqrt{24}$ then such a structure is equivalent to the ideal $Fm\bar{3}m$ unit cell with the lattice parameter $a\sqrt{2}$. If the length of c deviates from the "ideal" ratio the resulting structure has rhombohedral distortion.

At first we present our results on pure bulk CoO. Applying all three codes we found equilibrium lattice parameters, studied the DOS in optimized unit cells, computed the gap values and determined magnetic properties of CoO. A short summary of our studies of bulk CoO is shown in Table I. All the *ab initio* methods yield parameters of the CoO crystal which are close to those obtained previously both experimentally and theoretically. In all the cases, however, the GGA exchange-correlation functionals employed in *ab initio* methods cause a slight expansion of the lattice with respect to the experimental one.

The electronic structure of AF-II CoO was investigated in a number of works.[8,14,31,37] Briefly, the majority and the mi-

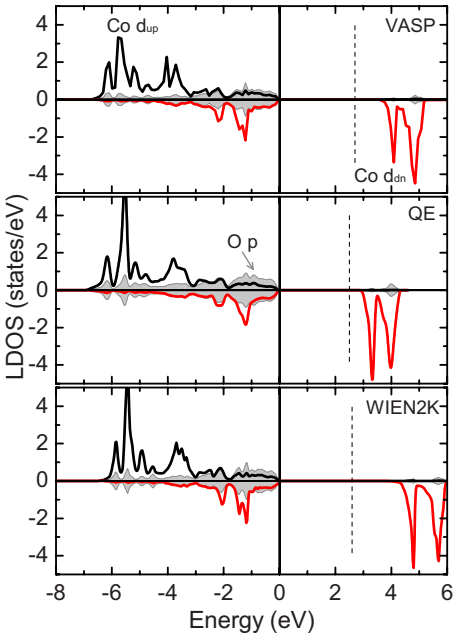

FIG. 2. (Color online) Spin-polarized PDOS of Co *d* (solid lines) and O *p* (shaded areas) states calculated by means of VASP, QE, and WIEN2K codes. The corresponding magnetic moments of Co atoms and gap values taken from the band structures (Fig. 3) are listed in Table I. Dashed lines point the edge of the gap.

nority states of the Co^{2+} ions are split due to the exchange interaction. Octahedral ligand field results in their further splitting into a triplet of t_{2g} states and a doublet of e_g states. High-spin configuration of Co^{2+} $3d$ electrons suggests that the majority orbitals are fully occupied but the minority t_{2g} states are filled with only two electrons. Majority states are hybridized with oxygen *p* states. Minority t_{2g} states are localized at the top of the valence band and are hybridized with *p* electrons of ligand oxygen. Strong correlational effects shift unoccupied minority t_{2g} and e_g states to higher energies, thus forming an insulating gap of 2.6 eV and hindering hybridization between these states and oxygen *p* states.[8,31]

All these features are seen in Fig. 2, which presents the results of our calculations. Partial DOS (PDOS) of Co *d* and O *p* electrons calculated by different methods are demonstrated. All three methods give very similar results relevant to the above-mentioned theoretical description but some code-dependent features can still be emphasized. Conduction-band edge which starts at the Fermi energy is marked in Fig. 2 by vertical stroked lines. To get physically correct values of the gap width we plotted the band structures of CoO and measure the energy difference between the highest valence band and the lowest conduction band. The band structure of CoO calculated by means of QE is presented in Fig. 3. Band structures obtained by means of VASP and WIEN2K are very similar. All the gap widths are very close to the experimental value (Table I). Despite of some differences in PDOS, spin magnetic moments of Co^{2+} ions are very similar in all three methods and vary from 2.60 to $2.77\mu_B$, which is in a good agreement with previous *ab initio* studies (Table I). Such moments are in reasonable agreement with the (2+) oxidation state of Co^{2+} ions. Note that experimentally measured magnetic moments of Co^{2+} ions are much higher due to the large orbital moment,[14,31] which is not calculated in our case. Oxygen ions are found to be nonmagnetic.

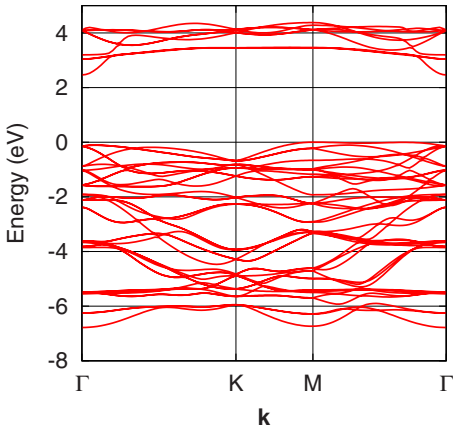

FIG. 3. (Color online) Band structure of CoO calculated along the Γ-K-M-Γ directions of the BZ of the hexagonal unit cell drawn in Fig. 1(a).

Summarizing this part, we can conclude that our description of the pristine bulk CoO by means of PP-PW codes is adequate and reasonably agrees with previous theoretical and experimental works as well as with our FP-LAPW calculations. Now we can turn to our results on doped CoO.

B. CoO doped with spin-flip Co impurity

The first impurity we dealt with was a Co atom with reversed magnetic moment, i.e., the magnetic moment of such an impurity is aligned antiparallel to the magnetic moments of Co in the same plane and parallel to the moments of Co in adjacent layers. QE calculations demonstrated that in the ideal supercell such a spin-flip perturbation is less favorable energetically by 166 meV than the unperturbed configuration. The sign of the interaction is quite expected. Indeed, let us analyze magnetic couplings in CoO within the simple Heisenberg model, described by the Hamiltonian[38,39]

$$\mathcal{H} = E_0 - \sum_{i,j;i\neq j} J_{i,j}(\mathbf{s}_i \cdot \mathbf{s}_j), \tag{6}$$

where E_0 is the energy of paramagnetic state, indexes *i* and *j* denote atoms in supercell and its translations whose interaction with each other cannot be neglected,[40] and $s_i = 3/2$ is the spin of a Co^{2+} ion. Every Co^{2+} ion in ideal $Fm\bar{3}m$ structure has 12 nearest-neighbor Co^{2+} ions (linked with solid lines in Fig. 4) and six next-nearest-neighbor Co^{2+} ions (linked with dashed lines in Fig. 4). Oxygen ligand atoms form a 90° angle between nearest-neighbor metal ions. We do not consider here the nature of nearest-neighbor exchange interaction and refer the reader to Ref. 39. It is important, that every Co^{2+} ion is coupled ferromagnetically to six nearest neighbors in the same {111} sheet and antiferromagnetically to six nearest neighbors in adjacent sheets. These contributions to Hamiltonian (6) cancel each other, so the AF-II order is established due to the magnetic coupling between the next-

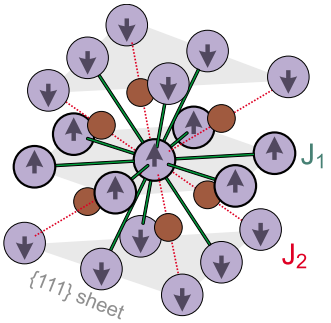

FIG. 4. (Color online) Co^{2+} ion is coupled with 12 first-nearest neighbors (J_1, green solid lines) and six next-nearest neighbors (J_2, red dashed lines).

nearest neighbors. Next-nearest neighbors form linear Co-O-Co configurations, thus making possible indirect superexchange interaction of strength J_2 between next-nearest Co^{2+} ions via intervening oxygen atoms. Physically it means that overlapped O p and two occupied Co t_{2g} orbitals acquire some energy gain in a singlet state.

We assume that all interactions except J_1 and J_2 are negligibly small, then Eq. (6) contains three unknown variables J_1, J_2, and E_0. Thus, to calculate exchange constants J_1 and J_2, one should consider at least three supercells with different magnetic configurations. Since we study properties of a *single impurity* it would be better to avoid bulk perturbations like the ferromagnetic supercell or supercells with another magnetic order. Two magnetic configurations in our case are an obvious choice: an unperturbed supercell with unbroken AF-II magnetic order and a supercell with one Co spin-flip impurity. Total energies $E_{\text{AF-II}}$ and $E^f_{\text{AF-II}}$ of these configurations give us $J_2=(E_{\text{AF-II}}-E^f_{\text{AF-II}})/(24s^2)=-3.1$ meV. The third configuration contains a nearest-neighbor pair of spin-flip impurities with the total energy $E^{2f}_{\text{AF-II}}$ and $J_1=(E_{\text{AF-II}}-2E^f_{\text{AF-II}}+E^{2f}_{\text{AF-II}})/(2s^2)=-2.0$ meV. These energies are similar to previously calculated values of $J_1=-1.6$ meV and $J_2=-1.46$ meV, which were derived by Harrison from the tight-binding formalism.[39]

Cell distortion affects both J_1 and J_2. A contraction along **c** axis results in a small reduction in the ion-oxygen distance, so the superexchange coupling constant J_2 should become higher. Due to the break of the symmetry the coupling constant between first-nearest neighbors in the same {111} plane is not equal anymore to the coupling constant to the first-nearest neighbors in adjacent {111} planes. Changes, however, are negligibly small: the spin flip causes an energy increase of 165 meV (vs 166 meV in the ideal supercell).

C. CoO doped with transition metal impurities

GGA+U calculations often converge to metastable electronic configurations corresponding to local minima of the total energy, so it is necessary to verify the results in order to avoid misleading artificial features in the electronic structure.[37] At first we would like to convince the reader that we really deal with transition metal (TM) impurities in a (2+) oxidation state. The simplest way to do this is to look at the magnetic moments of impurities. Figure 5 presents

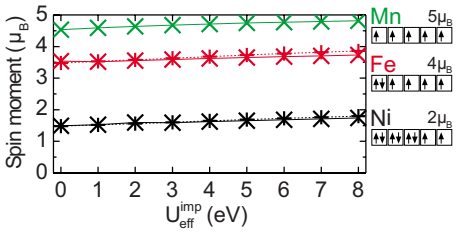

FIG. 5. (Color online) Magnetic moments of Mn, Fe, and Ni impurities in the ideal CoO supercell calculated by means of QE (×) and VASP (+). U^{imp}_{eff} is the screened Coulomb interaction at the impurity site. The corresponding fully localized high-spin configurations and their magnetic moments are listed on the right. We were not able to obtain the converged solution for Mn impurity by means of VASP.

a diagram of spin magnetic moments of TM =(Mn, Fe, and Ni) embedded into the ideal CoO supercell calculated by means of QE and VASP as a function of U^{TM}_{eff}. The d-shell high-spin configurations given on the right side show the impurity (2+) oxidation state. Magnetic moments deduced from these fully localized high-spin configurations are listed above configuration schemes. It is obvious that *ab initio* values plotted in Fig. 5 are in reasonable agreement with fully localized spin configurations.[37]

1. Ni^{2+} impurity

Ni has one additional electron in the $t_{2g}\downarrow$ orbital in comparison to Co. The PDOS calculated for Ni^{2+} by means of QE ($U^{\text{Ni}}_{eff}=4.5$ eV) and VASP ($U^{\text{Ni}}_{eff}=6.1$ eV) codes are plotted in Figs. 6(a) and 6(b), respectively. Both codes yield similar results. There are no impurity-induced states in the gap. The additional electron is situated below the Fermi energy and the whole density of occupied minority electrons is shifted downwards in comparison with pure CoO (Fig. 2). The reason for this effect is related to the exchange splitting of Ni, which is smaller than that of Co. To demonstrate this effect we plot in Figs. 6(a) and 6(b) d-PDOS calculated for Ni^{2+} in NiO but with the lattice constant of optimized CoO (Table I). The result obtained in VASP [Fig. 6(b)] matches the impurity d-PDOS and the smaller exchange splitting can be observed. The d-PDOS produced in QE at $U^{\text{Ni}}_{eff}=4.5$ eV is shifted to lower energies by $\simeq 1$ eV with a very narrow-gap width less than 1 eV [dashed blue curve in Fig. 6(a)]. Such a striking difference is explained by the overestimated U^{Ni}_{eff}. Indeed, contraction of NiO increases bonding between Ni and O and description of the system by means of the band theory becomes more relevant than a Hubbard-type description. This results effectively in a decrease in U^{Ni}_{eff}. To reinforce this statement we plot within Fig. 6(a) the d-PDOS calculated with $U^{\text{Ni}}_{eff}=4.2$ eV as a shaded area. The agreement with the d-PDOS of the impurity becomes feasible. Different behaviors of QE and VASP are explained by different types of pseudopotentials and different strategies used for calculation of occupation numbers. As we see further by the examples of Fe and Mn, expansion of the oxide lattice constant does not affect the value of U_{eff}.

For all the examined values of U^{Ni}_{eff}, Ni^{2+} is coupled to the CoO host without spin flip, i.e., Ni^{2+} is coupled ferromag-

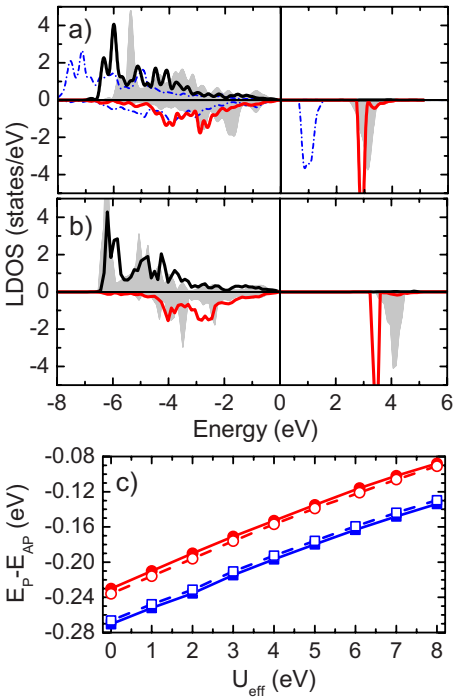

FIG. 6. (Color online) Spin-polarized *d*-PDOS at Ni^{2+} impurity embedded into the CoO supercell calculated with (a) QE and (b) VASP for U_{eff}^{Ni}=4.5 eV and U_{eff}^{Ni}=6.1 eV, respectively. Shaded gray areas in (a) and (b) represent the *d*-PDOS of NiO with CoO lattice structure calculated for U_{eff}^{Ni}=4.2 eV and U_{eff}^{Ni}=6.1 eV, respectively. Blue dashed curve in (a) corresponds to the *d*-PDOS of NiO with optimized CoO lattice constant at U_{eff}^{Ni}=4.5 eV. Panel (c) demonstrates exchange coupling of Ni^{2+} to CoO host calculated for various U_{eff}^{Ni} by means of QE (blue color, ■—ideal cell, □—distorted cell) and VASP (red color, ●—ideal cell, ○—distorted cell).

netically to the Co^{2+} ions in the same {111} sheet and antiferromagnetically to Co^{2+} ions in adjacent planes. The exchange energies calculated by means of QE and VASP for ideal and distorted cells are plotted in Fig. 6(c). It can be seen that distortions have minor effect on the value of exchange energies. Additionally, completely relaxed geometries were calculated by means of VASP and relaxations of the structure induced by the impurity were found to be negligibly small.

2. Fe^{2+} *impurity*

Fe stands in the periodic table just one atomic number before Co and therefore has one minority *d* electron less. The PDOS for Fe^{2+} calculated by means of QE and VASP for U_{eff}^{Fe}=4.5 eV is demonstrated in Figs. 7(a) and 7(b). The exchange splitting of Fe is larger than for Co, so the energy of the only occupied $t_{2g}\downarrow$ electron is shifted to the Fermi energy. Calculations for the FeO with the CoO lattice constant (Table I) give the *d*-PDOS, which is very close to the *d*-PDOS of the Fe^{2+} impurity. Similarly to Ni^{2+}, Fe^{2+} is coupled to the host CoO without a spin flip as it is demonstrated in Fig. 7(c). The appropriate self-consistent solution for the expanded FeO could not be found by means of VASP.

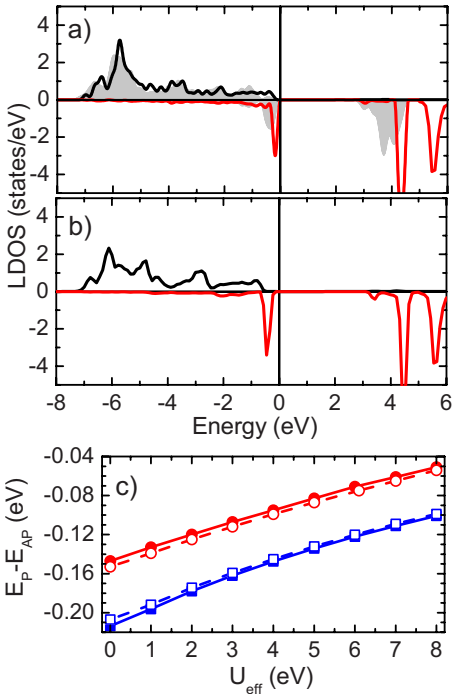

FIG. 7. (Color online) [(a)–(c)] Same as Fig. 6 but for Fe^{2+} impurity. U_{eff}^{Fe}=4.5 eV is used in (a) and (b).

3. Mn^{2+} *impurity*

The electronic configuration of Mn^{2+} *d* shells is $[(e_g\uparrow)^2(t_{2g}\uparrow)^3]$, i.e., there are no minority electrons in the valence band. The PDOS for Mn^{2+} for U_{eff}^{Mn}=4.5 eV, shown in Fig. 8(a), reflects this fact. The density of majority states is shifted toward the Fermi energy with respect to the PDOS of CoO (Fig. 2). A localized majority feature appears right below the Fermi level. The shape of Mn PDOS is well reproduced in the calculations of the MnO shrunk to match the CoO lattice constant [plotted in Fig. 8(a) with shaded areas].

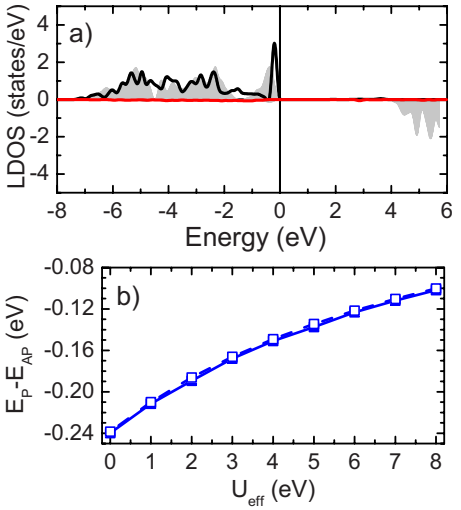

FIG. 8. (Color online) (a) *d*-PDOS calculated by means of QE at Mn^{2+} site for U_{eff}^{Mn}=4.5 eV. (b) Exchange coupling of Mn^{2+} impurity to CoO as a function of U_{eff} calculated by means of QE. Curve notation is the same as in Fig. 6.

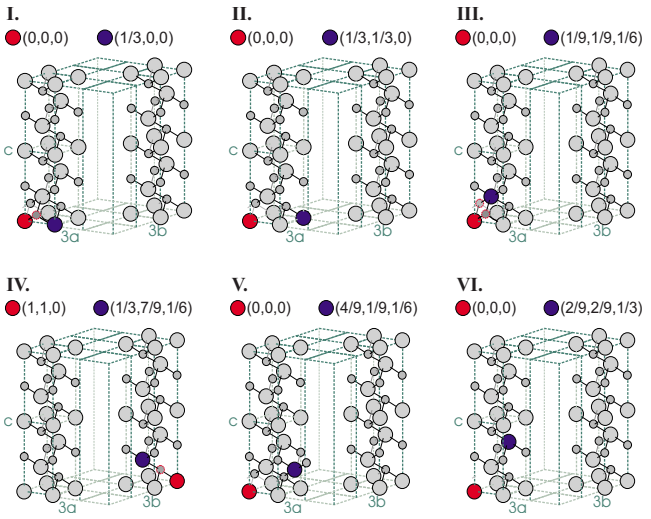

FIG. 9. (Color online) Sketches of mutual positions of two impurities in the supercell. Coordinates of both impurities in Bravais vectors of supercell are written at the top of each sketch.

Mn^{2+} ion is coupled to CoO without a spin flip as follows from the data presented in Fig. 8(b). We were not able to obtain the converged solution for Mn impurity by means of VASP.

4. Discussion

Monoxides of Ni, Fe, and Mn are similar to CoO: they also have $Fm\bar{3}m$ NaCl structure and the AF-II magnetic order[8,14] caused by the superexchange interaction of fully occupied majority $[(e_g\uparrow)^2(t_{2g}\uparrow)^3]$ states of metal ions via oxygen ions.[39] The lattice constant of NaCl TMO gradually decreases from MnO (a=4.445 Å) to NiO (a=4.171 Å).[14] Contraction of metal-oxygen bond results in the stronger superexchange interaction and, as a result, the Néel temperature rises with the atomic number of the TM. In our case the situation is somewhat different: the lattice and the bonds are fixed by the host CoO structure. Another delicate point is the choice of the Coulomb correlation energy U_{eff}^{TM}. To circumvent it we performed calculations for a set of $U_{eff}^{\mathrm{TM}} \in [0,\ldots,8]$ eV as it is shown in Figs. 6(c), 7(c), and 8(b).

The exchange energy of Mn, Fe, and Ni exhibits the same trend: it is strongest at $U_{eff}^{\mathrm{TM}}=0$ eV and then gradually decreases in the interval $[0,\ldots,8]$ eV by $\simeq$100 meV. VASP and QE give different but still comparable values for Ni and Fe impurities. The exchange coupling of Ni^{2+} and Fe^{2+} ions to the host CoO obtained by means of VASP is smaller than the values calculated by means of QE both for ideal and distorted supercells. Relaxations play a minor role as was proven by VASP calculations.

IV. PAIRS OF IMPURITIES

Finally we present our results for pairs of impurities. We chose pairs of Mn^{2+}, Fe^{2+}, and Ni^{2+} impurities and embedded them into various positions in ideal and distorted supercells. Our primary goal was to study the possibility of the ferromagnetic ordering of impurities in these systems. The next question we addressed was the possibility of clustering of impurities at low concentrations.

The considered configurations are sketched in Fig. 9 together with coordinates of both impurities in units of Bravais vectors of the supercell. The magnetic moment of the first impurity at (0,0,0) is always aligned parallel to the magnetic moments of cobalt atoms in the same {111} sheet. Two opposite alignments ($\uparrow\uparrow$ and $\uparrow\downarrow$) of the magnetic moment of the second impurity are considered in order to find the exchange energy $E_{\uparrow\downarrow}=E_{\uparrow\uparrow}-E_{\uparrow\downarrow}$ of the pair. Values of $E_{\uparrow\downarrow}$ calculated for configurations I–VI are listed in Table II. One can see that all the considered impurities (Mn^{2+}, Fe^{2+}, and Ni^{2+}) follow the magnetic order of the host material, i.e., their magnetic moments are always coaligned with moments of Co in the same {111} sheet. This fact speaks against the possibility of the ferromagnetic ordering in such kind of systems at low concentration of impurities.[21]

To study clustering we compared total energies of considered configurations. The total energy $E_{Tot}^{\mathrm{I}}=\min(E_{\uparrow\uparrow}^{\mathrm{I}},E_{\uparrow\downarrow}^{\mathrm{I}})$ of configuration I (Fig. 9) was chosen as a relative zero. The total energies $E_{Tot}^{C}=\min(E_{\uparrow\uparrow}^{C},E_{\uparrow\downarrow}^{C})-E_{Tot}^{\mathrm{I}}$ of all the configurations C=(I–IV) are listed in Table II with respect to this value. It is clear that total energies of all the configurations are approximately equal and, thus, cannot promote clustering without significant distortion of the host NaCl crystal structure. Similar conclusion has recently been made for Fe impurities in NiO.[21]

TABLE II. Exchange $E_{\uparrow\downarrow}$ and relative total E_{Tot} energies of a pair of impurities in configurations sketched in Fig. 9. Exchange energies of single impurities with CoO host are listed in the column "single" for the sake of comparison. Results obtained for distorted supercell are placed in brackets.

		Configurations						
		I	II	III	IV	V	VI	Single
Mn	$E_{\uparrow\downarrow}$ (meV)	−165 (−177)	−141 (−145)	161 (166)	131 (134)	145 (148)	−144 (−147)	−144 (−143)
U_{eff}^{Mn}=4.5 eV	E_{Tot} (meV)	0 (0)	19 (0)	21 (19)	4 (2)	22 (20)	21 (19)	
Fe	$E_{\uparrow\downarrow}$ (meV)	−130 (−131)	−141 (−141)	140 (141)	135 (135)	142 (141)	−141 (−141)	−141 (−140)
U_{eff}^{Fe}=4.5 eV	E_{Tot} (meV)	0 (0)	9 (8)	11 (9)	5 (4)	10 (8)	9 (8)	
Ni	$E_{\uparrow\downarrow}$ (meV)	−186 (−188)	−187 (−189)	187 (187)	192 (193)	187 (188)	−187 (−188)	−188 (−184)
U_{eff}^{Ni}=4.5 eV	E_{Tot} (meV)	0 (0)	−4 (−3)	−3 (−4)	−8 (−8)	−4 (−4)	−3 (−4)	

V. CONCLUSIONS

In conclusion, we have studied, by means of the GGA $+U$, the rocksalt CoO with the AF-II antiferromagnetic structure and the magnetic states of transition metal impurities incorporated in it. State-of-the-art *ab initio* codes have been applied for calculations of lattice parameters, electronic structure, and magnetic properties of pure CoO. A systematic investigation of transition metal impurities (Mn, Fe, and Ni) incorporated into the CoO has been performed. We have studied the changes in the strength of the exchange coupling of impurities to the host depending on the parameter U_{eff}. Obtained results are found to be slightly affected by the choice of U_{eff}. We have revealed that Mn, Fe, and Ni impurities do not form small clusters and do not break the AF-II magnetic order of the host CoO.

ACKNOWLEDGMENTS

This work has been supported by the Deutsche Forschungsgemeinschaft Sonderforschungsbereich SFB 762.

[1] C. N. R. Rao, *Transition Metal Oxides: Crystal Chemistry, Phase Transition and Related Aspects* (Indian Institute of Technology Kharagpur, United States National Bureau of Standards, Washington, DC, 1974), pp. 54–78.
[2] M. Gvishi and D. Tannhauser, J. Phys. Chem. Solids **33**, 893 (1972).
[3] J. Zaanen, G. A. Sawatzky, and J. W. Allen, Phys. Rev. Lett. **55**, 418 (1985).
[4] S. Hüfner, Adv. Phys. **43**, 183 (1994).
[5] K. Terakura, T. Oguchi, A. R. Williams, and J. Kübler, Phys. Rev. B **30**, 4734 (1984).
[6] T. C. Leung, C. T. Chan, and B. N. Harmon, Phys. Rev. B **44**, 2923 (1991).
[7] P. Dufek, P. Blaha, V. Sliwko, and K. Schwarz, Phys. Rev. B **49**, 10170 (1994).
[8] V. I. Anisimov, J. Zaanen, and O. K. Andersen, Phys. Rev. B **44**, 943 (1991).
[9] M. T. Czyżyk and G. A. Sawatzky, Phys. Rev. B **49**, 14211 (1994).
[10] V. I. Anisimov, F. Aryasetiawan, and A. I. Lichtenstein, J. Phys.: Condens. Matter **9**, 767 (1997).
[11] A. I. Liechtenstein, V. I. Anisimov, and J. Zaanen, Phys. Rev. B **52**, R5467 (1995).
[12] S. L. Dudarev, G. A. Botton, S. Y. Savrasov, C. J. Humphreys, and A. P. Sutton, Phys. Rev. B **57**, 1505 (1998).
[13] M. Cococcioni and S. de Gironcoli, Phys. Rev. B **71**, 035105 (2005).
[14] F. Tran, P. Blaha, K. Schwarz, and P. Novák, Phys. Rev. B **74**, 155108 (2006).
[15] P. Gopal and N. A. Spaldin, Phys. Rev. B **74**, 094418 (2006).
[16] K. Potzger, S. Zhou, H. Reuther, A. Mücklich, F. Eichhorn, N. Schell, W. Skorupa, M. Helm, J. Fassbender, T. Herrmannsdörfer, and T. P. Papageorgiou, Appl. Phys. Lett. **88**, 052508 (2006).
[17] C. Song, X. J. Liu, K. W. Geng, F. Zeng, F. Pan, B. He, and S. Q. Wei, J. Appl. Phys. **101**, 103903 (2007).
[18] C. D. Pemmaraju, R. Hanafin, T. Archer, H. B. Braun, and S. Sanvito, Phys. Rev. B **78**, 054428 (2008).
[19] L. M. Sandratskii and P. Bruno, Phys. Rev. B **73**, 045203 (2006).
[20] T. Wolfram and S. Ellialtigolu, *Electronic and Optical Properties of d-Band Perovskites* (Cambridge University Press, Cambridge, 2006).
[21] J. H. He, S. L. Yuan, Y. S. Yin, Z. M. Tian, P. Li, Y. Q. Wang, K. L. Liu, and C. H. Wang, J. Appl. Phys. **103**, 023906 (2008).
[22] A. B. Shick, A. I. Liechtenstein, and W. E. Pickett, Phys. Rev. B **60**, 10763 (1999).
[23] G. Kresse and J. Hafner, Phys. Rev. B **47**, 558 (1993).
[24] G. Kresse and J. Furthmüller, Phys. Rev. B **54**, 11169 (1996).
[25] G. Kresse and D. Joubert, Phys. Rev. B **59**, 1758 (1999).
[26] S. Baroni, A. Dal Corso, S. de Gironcoli, and P. Giannozzi, 2005, PWSCF and PHONON: plane-wave pseudopotential codes http://www.pwscf.org/
[27] S. Baroni, A. Dal Corso, S. de Gironcoli, and P. Giannozzi, 2005, QUANTUM ESPRESSO: open-source package for research in electronic structure, simulation, and optimization http://www.quantum-espresso.org/
[28] P. Blaha, K. Schwarz, G. K. H. Madsen, D. Kvasnicka, and J. Luitz, *WIEN2K: An Augmented Plane Wave and Local Orbitals Program for Calculating Crystal Properties* (Vienna University of Technology, Austria, 2001).
[29] H. J. Monkhorst and J. D. Pack, Phys. Rev. B **13**, 5188 (1976).
[30] Y. Wang and J. P. Perdew, Phys. Rev. B **44**, 13298 (1991); J. P. Perdew, J. A. Chevary, S. H. Vosko, K. A. Jackson, M. R. Pederson, D. J. Singh, and C. Fiolhais, *ibid.* **46**, 6671 (1992); J. P. Perdew, in *Electronic Structure of Solids'91*, edited by P. Ziesche and H. Eschrig (Akademie, Berlin, 1991).
[31] U. D. Wdowik and K. Parlinski, Phys. Rev. B **75**, 104306 (2007).
[32] J. P. Perdew, K. Burke, and M. Ernzerhof, Phys. Rev. Lett. **77**, 3865 (1996).
[33] P.-O. Löwdin, J. Chem. Phys. **18**, 365 (1950).
[34] M. Methfessel and A. T. Paxton, Phys. Rev. B **40**, 3616 (1989).
[35] W. Jauch, M. Reehuis, H. J. Bleif, F. Kubanek, and P. Pattison, Phys. Rev. B **64**, 052102 (2001).
[36] W. Jauch and M. Reehuis, Phys. Rev. B **65**, 125111 (2002).
[37] W. Zhang, K. Koepernik, M. Richter, and H. Eschrig, Phys. Rev. B **79**, 155123 (2009).
[38] C. Kittel, *Introduction to Solid State Physics*, 7th ed. (Wiley, New York, 1996).
[39] W. A. Harrison, Phys. Rev. B **76**, 054417 (2007).
[40] Note, that pairs ij and ji are equivalent, and very often, in order to avoid double summation, Heisenberg Hamiltonian is written down with factor 1/2 or with summation is performed over inequivalent pair ij.